Journal of Solid State Electrochemistry (2023) 27:255–270
https://doi.org/10.1007/s10008-022-05315-7

ORIGINAL PAPER

Glutathione as green corrosion inhibitor for 6061Al-SiC$_{(p)}$ composite in HCl medium: electrochemical and theoretical investigation

Unnimaya[1] · Prakasha Shetty[1] · Preethi Kumari[1] · Sneha Kagatikar[1]

Received: 4 March 2022 / Revised: 1 September 2022 / Accepted: 19 October 2022 / Published online: 2 November 2022

Abstract

This research deals with the inhibition activity of glutathione in 0.5 M HCl on the corrosion behavior of 6061Al-SiC$_{(p)}$ composite. Glutathione is an eco-friendly water-soluble inhibitor. Polarization results reveal the cathodic inhibitor behavior of glutathione (Gt). The inhibition performance of Gt increases by increasing its concentration and lowering the medium temperature. The decrease in the corrosion current density and increase in inhibition efficiency on increasing Gt concentration reveal the attenuation of composite corrosion. Experimental results indicate the mixed adsorption with predominantly physisorption of Gt molecules adsorption on the composite surface following Langmuir adsorption isotherm. The impedance measurements indicate the rise in polarization resistance with an increase in Gt concentration, showing the control of composite corrosion. The surface analysis of the corroded and inhibited composite samples using a scanning electron microscope and atomic force microscope supports Gt molecules' adsorption. The quantum chemical calculations confirm the conclusions of the experimental studies.

Keywords Acid corrosion · 6061Al-SiC(p) · Electrochemical methods · Glutathione · Physisorption

Introduction

The deterioration of materials (such as metals, alloys, and composites) through chemical or electrochemical interaction with the environment is known as corrosion. It mainly results in adverse effects such as loss of materials, plant shutdown that leads to production loss, increased maintenance cost, oil leakage due to pipeline breakage, contamination of products because of metal leaching, and environmental pollution [1]. The estimated cost of corrosion worldwide is increasing drastically, indicating the significance of corrosion control in conserving the world's material resources. Metal matrix composites (MMCs) are novel structural materials because of their lightweight, environmental resistance, and favorable mechanical properties. MMCs composed of two phases, the matrix phase and the dispersed phase. Aluminum alloys are the commonly used metal matrix materials reinforced with various particulate or fiber materials [2]. In 6061Al-SiC composite, 6061Al alloy is the matrix phase, reinforced with SiC particulate. These composites with high specific strength, ideal for vehicles, aircraft, and military applications [3]. Adding ceramic particles, short fibers, and whiskers to aluminum alloys improves tribological characteristics significantly. A metal matrix alloy is usually less prone to corrosion than the corresponding MMC. The presence of reinforcing particles or fibers causes in-homogeneities on surfaces exposed to aggressive environments. It becomes significant in MMCs made of aluminum alloy matrix and semiconductor-type reinforcing materials such as silicon carbide. In such cases, the galvanic cell formation promotes the corrosion of the metal matrix [4]. The HCl solution is widely used in the automobile and aero industry pickling processes, where the excessive degradation of the materials should be adequately controlled.

Thus, the corrosion of MMCs such as 6061Al-SiC$_{(p)}$ composite in an aggressive medium like hydrochloric acid solution can be best controlled using a suitable inhibitor. Combating corrosion by the addition of inhibitors is the easiest and simplest method. As per the literature, organic compounds with heteroatoms and conjugate double bonds act as effective inhibitors to combat the corrosion of many metals [5, 6]. Amino acids are employed as environment-friendly

✉ Prakasha Shetty
prakash.shetty@manipal.edu; dr.shetty60@rediffmail.com

[1] Department of Chemistry, Manipal Institute of Technology, Manipal Academy of Higher Education, Manipal 576104, Karnataka, India

inhibitors to combat many metals' deterioration [7]. Glutathione is an amino acid derivative containing multiple heteroatoms (sulfur, oxygen, and nitrogen), polar groups (−CO, $-NH_2$, −OH), and conjugated double bonds in their structures (Fig. 1), expected to show good inhibition activity. It is a non-toxic material readily soluble in an aqueous medium. Glutathione exhibited a good inhibition efficiency towards copper [8] and AA6061 [9] in the hydrochloric acid medium. This paper demonstrates the inhibition behavior of an eco-friendly inhibitor, glutathione, on the attenuation of 6061 Al- $SiC_{(p)}$ composite corrosion in a 0.5 M HCl solution. The surface morphology of corroded and inhibited composite specimens was analyzed. UV–visible and FTIR spectral analysis supported the adsorption of Gt molecules on the composite surface. Experimental results were compared with the results of the theoretical calculations.

Materials and methods

Materials

The specimen employed in the present work is 6061Al-15% $_{(v)}$ $SiC_{(p)}$ composite (hereafter referred to as Al alloy-SiC). Its elemental composition is mentioned in Table 1.

The specimen was obtained by cutting a cylindrical rod of the material, and then, it was embedded in an epoxy resin, exposing the surface area of 1 cm^2. The specimen's exposed surface was abraded using different grades (200–1000) of emery paper and finally on a disc polisher. Then, the sample was washed thoroughly with water, acetone rinsed, and finally dried. The corrosive medium used in this study is 0.5 M HCl, prepared using 35% HCl (analar grade) and standardized volumetrically. Glutathione (Merck) is the inhibitor. Figure 1 depicts the structure of glutathione (Gt).

Electrochemical studies

The experimental studies were performed using a CH instrument (604D series USA model with beta software). The study was done at four different temperatures (303, 313, 323, and 333 K) using a cell system comprising an auxiliary electrode of platinum, a reference electrode of saturated calomel, and a working electrode of an Al alloy-SiC composite specimen. Initially, the cell system was immersed in a 100 ml of 0.5 M HCl solution contained in a beaker and connected to the CH instrument. The setup is kept for about 1 h to attain the steady-state condition, and then, the open circuit potential (OCP) is recorded. First, the electrochemical impedance studies (EIS) were performed in the frequency range, 10 kHz–0.01 Hz, under an applied AC signal of 10 mV amplitude by varying the concentration of Gt. The potentiodynamic polarization (PDP) studies were done by polarizing the working electrode at OCP from −250 mV (cathodic) to +250 mV (anodic) with a scan rate of 1 mVs^{-1}. Then, the Tafel curves were recorded. Three trials were taken in each measurement, and the average value was used for further calculations.

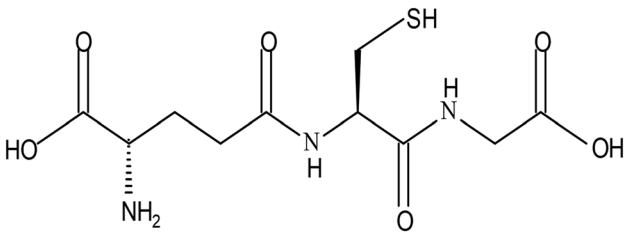

Fig. 1 The structure of glutathione (Gt)

Table 1 The composition of Al alloy-SiC composite

Elements	Mg	Si	Cu	Cr	Al
Composition (wt.%)	0.60	1.0	0.02	0.01	98.37

Surface studies of the composite specimen

The composite specimen was subjected to surface studies to identify the surface texture of the corroded and inhibited samples. The surface pictures of the composite sample immersed in a solution of 0.5 M HCl without and with Gt, respectively, for 3 h were taken using EVO 18-5-57 model SEM. The surface roughness of these composite samples was checked using AFM (IB342 Innova model).

UV–visible and FTIR study on the adsorption of Gt

Using an 1800 Shimadzu UV–visible spectrophotometer, UV–visible spectra of 0.1 mM Gt in 0.5 M HCl solution were initially recorded. The absorption spectra of the same solution were then recorded after 2 h of immersion of the test coupon of AA-SiC composite.

FTIR spectroscopy was performed on scrapped products produced after immersion of the composite specimen in 0.1 mM Gt in 0.5 M HCl solution for 2 h using Shimadzu-IR Spirit in the frequency range 4000–400 cm^{-1}.

Theoretical simulation studies

The experimental results of the inhibition activity of Gt were validated through the theoretical studies using density functional theory (DFT) with the help of 6-31G** as the basis set and B3LYP as the exchange–correlation function. The

computed parameters were analyzed for the validation of the electrochemical results.

Result and discussion

Open circuit potential (OCP)

The OCP monitoring is essential for all corrosion studies since electrochemical techniques like EIS work at OCP and potentiodynamic polarization are accomplished by drifting the system away from its equilibrium state. In both circumstances, OCP plays a critical role, and if it were not maintained, the accuracy of the electrochemical result would affect. To establish a steady state, the freshly polished composite specimen was dipped in 0.5 M HCl in the absence and presence of Gt. The change in electrode potential with time was recorded. As shown in Fig. 2, the test specimen reached the steady-state potential in 0.5 M HCl in the presence and absence of Gt in around 1500 s. As seen in Fig. 2, the potential first changes to a critical value known as the induction time. Upon visual inspection, a dull layer could be seen on the specimen electrode surface. This dull coating could be attributable to surface corrosion products or oxide layer deposition [10]. After the initial induction period, the potential reaches a steady state, implying the attainment of a dynamic equilibrium between surface film deposition and underlying metal dissolution via surface film breakdown or dissolution. In the presence of Gt, the potential values shift towards the cathodic area, indicating that the inhibitor primarily affects the cathodic reaction. EIS and potentiodynamic polarization measurements were performed after establishing the OCP.

Potentiodynamic polarization studies

The Tafel plots for Al alloy-SiC composite in the acid and inhibited acid medium at 303 K are depicted in Fig. 3.

Similar curves were obtained at 313, 323, and 333 K also. The anodic curve is accountable for metal oxidation, while the cathodic curve is responsible for hydrogen evolution in the acidic medium [11]. Table 2 presents the electrochemical parameters for the composite, such as corrosion potential (E_{corr}), corrosion current density (i_{corr}), anodic Tafel slope (β_a), cathodic Tafel slope (β_c), and corrosion rate (CR) at various Gt concentrations and temperatures of the hydrochloric acid medium. The Tafel plots (Fig. 3) show that when the concentration of Gt rises, the anodic and cathodic curves shift to lower corrosion current densities (i_{corr}). In the presence of Gt, the corrosion potential (E_{corr}) shifts towards the cathodic region. However, the shift is less than ±85 mV, the widely accepted threshold for determining whether an inhibitor is exclusively anodic or cathodic [12]. The change in E_{corr} value corresponds to inhibitors' mixed-type behavior, controlling metal dissolution at the anode and hydrogen evolution at the cathode to various extents. However, the predominant control is on the cathodic hydrogen evolution reaction, reducing the overall rate of corrosion [13]. Besides these findings, the significant reduction in corrosion current density (i_{corr}) shows an effective decrease in corrosion rate in an optimal Gt concentration of 0.7 mM in a 0.5 M

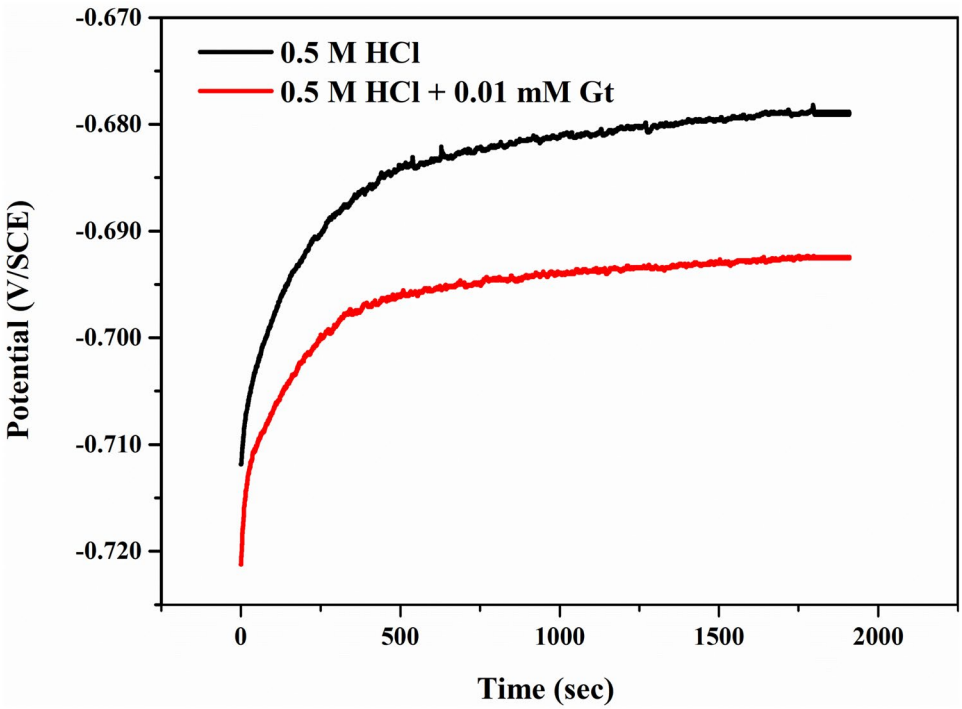

Fig. 2 Potential measurements of working electrode vs. SCE with time in the absence and presence of 0.01 mM Gt in 0.5 M HCl

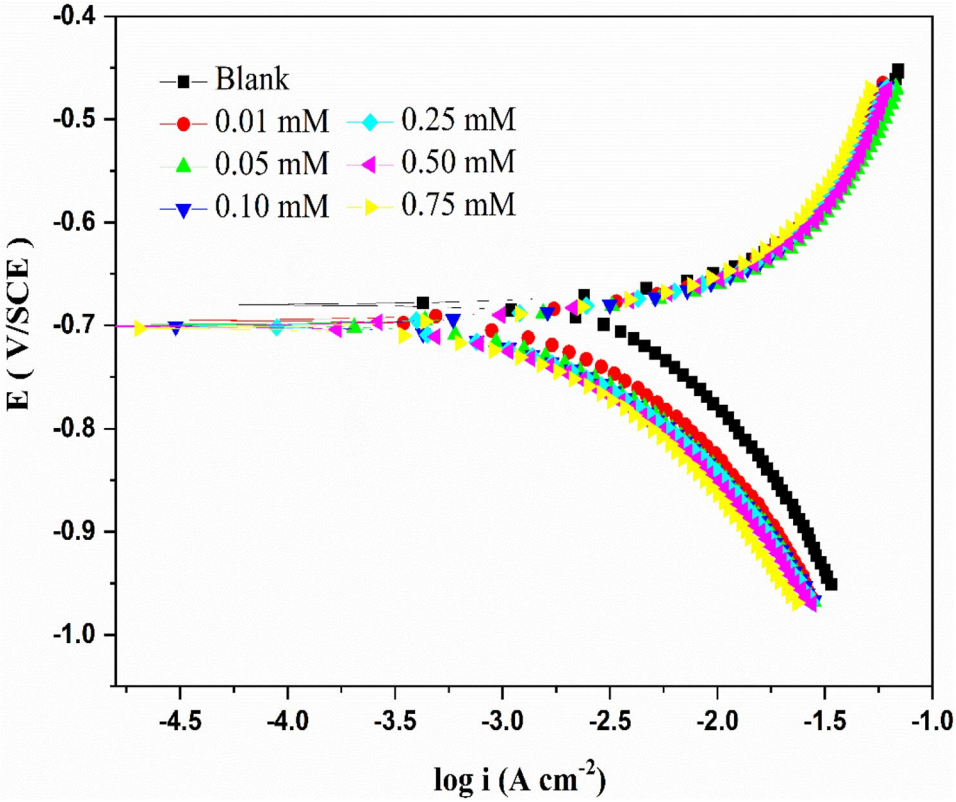

Fig. 3 Tafel plots for Al alloy-SiC composite in 0.5 M HCl without and with Gt at 303 K

hydrochloric acid medium. The results obtained at other temperatures are comparable to the one reported.

The inhibition efficiency, % *IE*, was calculated using Eq. (1).

$$\% IE = \frac{i_{corr} - i_{corr(inh)}}{i_{corr}} \times 100 \quad (1)$$

i_{corr} and $i_{corr(inh)}$ represent the corrosion current density in the corrosive medium without and with Gt, respectively [14].

In the presence of Gt, the values of i_{corr} decrease, increasing *IE*. It is presumably due to the film formation by Gt molecules adsorption, thereby protecting the composite from corrosion [15]. The observed anodic (β_a) and cathodic (β_c) slope values do not vary significantly in the inhibited solution and the acid medium, suggesting no change in the corrosion mechanism either in the acid or inhibited acid medium [16].

Electrochemical impedance spectroscopy (EIS) studies

EIS measurements were performed to access the Al alloy-SiC composite's deterioration in 0.5 M HCl containing varying concentrations of Gt. Figure 4 shows impedance plots for Al alloy-SiC composites at 303 K in varying Gt concentrations. From the impedance plot, it is clear that the depressed semicircle diameter increases on increasing the Gt concentrations, suggesting a decrease in corrosion rate. Due to inhomogeneity, such as the roughness of the specimen surface, the deposition of corrosion product, or the adsorption of Gt molecules, the impedance plots capacitive loops are depressed [17]. Similar plots were obtained at other temperatures also. Similar impedance plots have been reported in the literature on the control of corrosion of Al alloy and its composite in the hydrochloric acid media [18–20]. At a higher frequency, the impedance plot shows a capacitive loop and an inductive loop at a lower frequency. The higher frequency (HF) loop corresponds to the resistance offered for the charge transfer of the corrosion process, and the lower frequency (LF) loop to the relaxation process of hydrogen ions and the adsorption of corrosive chloride ions onto the oxide film [21]. The metal Al is oxidized to Al^+ ions and migrates to the oxide/electrolyte interface forming Al^{3+} ions. At the same time, O^{2-} or OH^- ions formed at the oxide/electrolyte interface. Due to the overlapping processes or one process dominating the others, all of these processes may be represented by a single capacitive loop [22]. In the presence of Gt, the area covered by the HF loop and LF loop combined is more than in its absence, which might be due to Gt forming a barrier film on the composite surface,

Table 2 PDP results for Al alloy-SiC composite in 0.5 M HCl without and with Gt at varying temperatures

T (K)	C_{Inh} (mM)	E_{corr} (V)	$-\beta_c$ (mV dec^{-1})	β_a (mV dec^{-1})	i_{corr} (mAcm^{-2})	CR (mmy^{-1})	% IE
303	blank	−0.680 ± 0.006	4.805	4.805	10.690 ± 0.09	118.70 ± 1.04	-
	0.01	−0.695 ± 0.004	5.997	5.176	4.807 ± 0.04	53.40 ± 0.50	55.03
	0.05	−0.699 ± 0.005	6.530	5.185	3.633 ± 0.03	40.38 ± 0.40	66.01
	0.10	−0.701 ± 0.004	6.630	5.372	2.685 ± 0.02	30.95 ± 0.29	74.88
	0.25	−0.700 ± 0.002	6.773	5.361	2.488 ± 0.02	27.63 ± 0.26	76.73
	0.50	−0.701 ± 0.003	6.761	5.684	2.292 ± 0.02	25.46 ± 0.25	78.56
	0.75	−0.703 ± 0.006	6.302	5.552	2.131 ± 0.02	23.67 ± 0.22	80.07
313	blank	−0.697 ± 0 004	4.825	4.905	14.380 ± 0.12	159.80 ± 1.30	-
	0.01	−0.700 ± 0.003	5.524	5.002	7.673 ± 0.07	85.26 ± 0.84	46.64
	0.05	−0.703 ± 0.005	6.059	5.159	5.738 ± 0.05	63.74 ± 0.61	60.10
	0.10	−0.707 ± 0.004	6.059	5.159	4.118 ± 0.04	45.74 ± 0.38	71.36
	0.25	−0.707 ± 0.006	6.199	5.368	3.750 ± 0.03	41.65 ± 0.40	73.92
	0.50	−0.707 ± 0.003	6.287	5.450	3.564 ± 0.03	39.60 ± 0.38	75.22
	0.75	−0.708 ± 0.004	6.374	5.078	3.192 ± 0.02	35.46 ± 0.36	77.80
323	blank	−0.705 ± 0.003	3.972	4.688	18.630 ± 0.18	203.75 ± 2.00	-
	0.01	−0.702 ± 0.005	5.432	4.810	11.100 ± 0.11	121.73 ± 1.10	40.42
	0.05	−0.705 ± 0.004	5.679	5.034	7.942 ± 0.07	86.12 ± 0.82	52.60
	0.10	−0.710 ± 0.005	5.779	5.247	6.585 ± 0.06	72.29 ± 0.71	64.65
	0.25	−0.713 ± 0.003	6.018	5.415	5.918 ± 0.06	64.70 ± 0.64	68.23
	0.50	−0.710 ± 0.004	6.043	5.416	5.491 ± 0.05	60.16 ± 0.60	70.53
	0.75	−0.714 ± 0.006	6.048	5.418	4.847 ± 0.04	53.43 ± 0.52	73.98
333	blank	−0.708 ± 0.006	4.872	4.675	22.85 ± 0.21	220.5 ± 2.06	-
	0.01	−0.710 ± 0.005	5.432	5.250	13.92 ± 0.12	134.3 ± 1.28	39.08
	0.05	−0.712 ± 0.005	5.679	5.024	11.74 ± 0.10	113.2 ± 1.12	48.62
	0.10	−0.711 ± 0.004	5.779	5.347	9.357 ± 0.08	90.25 ± 0.92	59.05
	0.25	−0.712 ± 0.004	6.018	5.515	8.370 ± 0.07	80.83 ± 0.82	63.37
	0.50	−0.713 ± 0.006	6.043	5.316	7.170 ± 0.06	69.18 ± 0.70	68.62
	0.75	−0.715 ± 0.006	6.048	5.218	6.372 ± 0.05	61.49 ± 0.62	72.11

influencing the processes as mentioned earlier [23]. In the presence of Gt, Fig. 4 clearly shows expanded capacitive and inductive loops, indicating increased corrosion resistance.

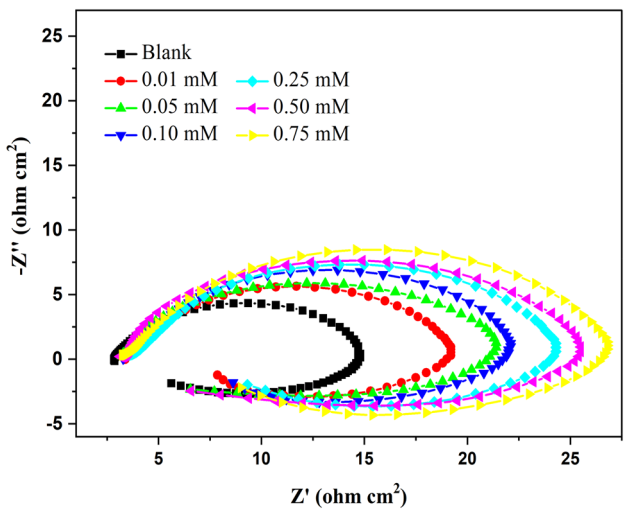

Fig. 4 Impedance plots for Al alloy-SiC composite in the acid and inhibited acid medium at 303 K

Due to ionic conduction in the oxide film, the aluminum oxide film is considered a parallel circuit of a resistor and a capacitor due to its dielectric characteristics [24, 25].

An appropriate equivalent circuit was obtained by simulating the EIS data for the composite in the presence of Gt in the acid medium using ZSimpWin software (version 3.21). The Nyquist plot was simulated using an equivalent electric circuit shown as an inset in Fig. 5 to fit the impedance obtained theoretically. The representative simulated and fitted curves for corrosion of the alloy composite in the presence of 0.75 mM Gt in 0.5 M HCl at 303 K are shown in Fig. 5.

In the equivalent circuit (Fig. 5), R_s represents the solution resistance, R_{ct} indicates the charge transfer resistance, and Q is the constant phase element (CPE) that corresponds to the capacitance (C) of the double layer. L is an inductive element, and R_L is the equivalent resistance. The elements R_s and R_{ct} are parallel in the circuit. Because the impedance plots show depressed semicircles, Q is substituted for actual capacitance C in simulation. Because of surface inhomogeneity, the frequency dispersion is accounted for during impedance analysis.

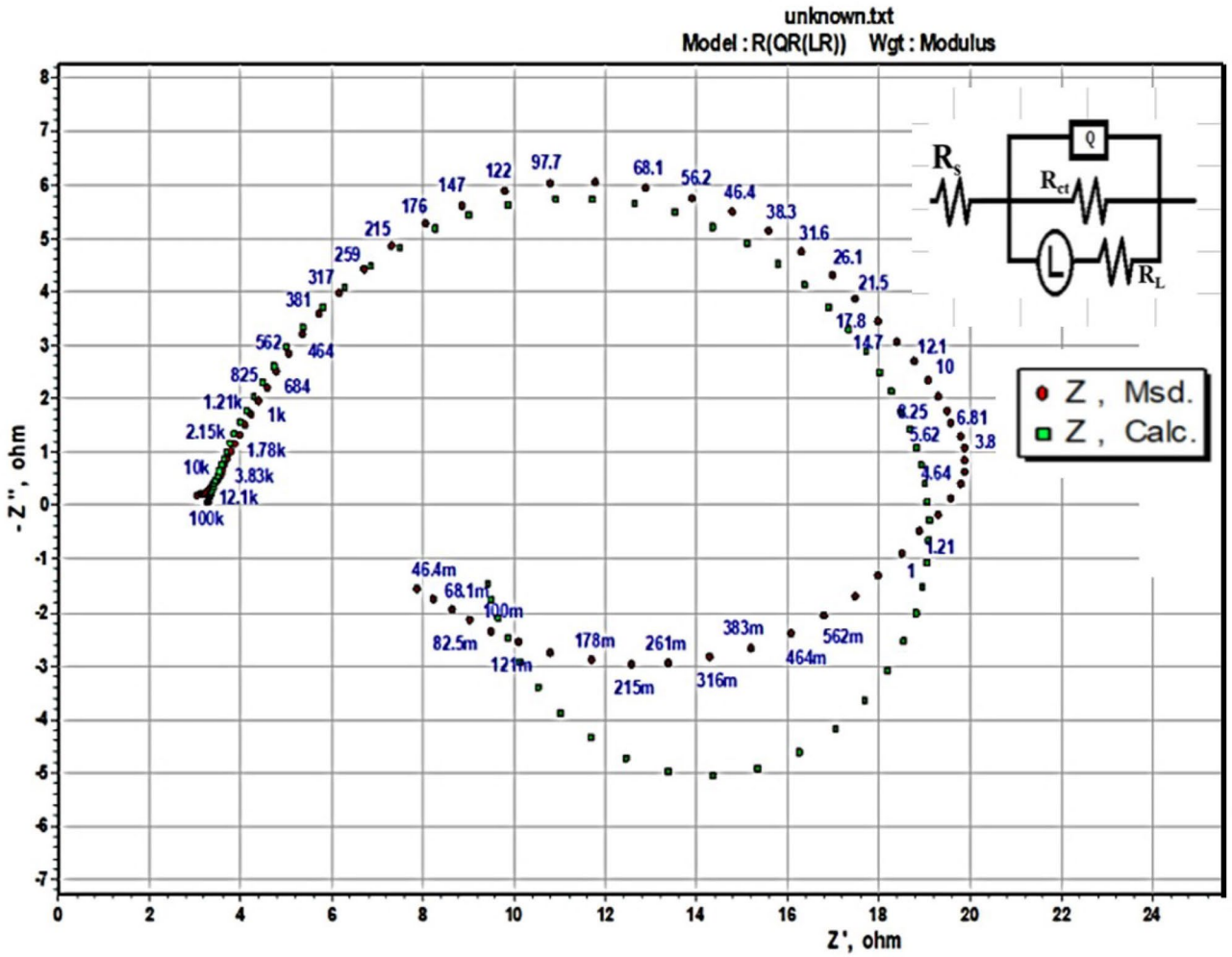

Fig. 5 The simulated plot and the equivalent circuit

Equation (2) was used to compute the double-layer capacitance (C_{dl}).

$$C_{dl} = Q_{dl}(2\pi f_{max})^{n-1} \tag{2}$$

where Q_{dl} is the *CPE* constant, f_{max} represents the frequency where the imaginary part of the impedance is maximum, and n is the *CPE* exponent related to the surface morphology of the composite electrode surface and lies in the range $-1 \le n \le 1$. When $n = 1$, *CPE* acts as an ideal capacitor [26].

The polarization resistance (R_p) is computed from Eq. (3) [18].

$$R_p = \frac{R_{ct}R_L}{R_{ct} + R_L} \tag{3}$$

Based on the polarization values in the blank (R_p) and inhibited medium ($R_{p(inh)}$), the percentage *IE* can be calculated using Eq. (4) [18].

$$\%\ IE = \frac{R_{p(inh)} - R_p}{R_{p(inh)}} \times 100 \tag{4}$$

From Table 3, it is clear that the value of R_p increases with the Gt concentrations, resulting in improved corrosion resistance in the presence of Gt. Because of film formation by Gt on the composite surface, higher resistance is offered for the flow of electrons, resulting in the reduction of corrosion rate and increase of *IE* [27]. The decrease in C_{dl} value (Table 3) observed in increasing Gt concentrations is probably due to the rise in the electrical double-layer thickness at the composite/solution interface [28]. These findings are supported by an increase in the percentage of *IE* with increasing Gt concentrations. The experimental results obtained at other temperatures showed similar patterns.

Table 3 EIS parameters for Al alloy-SiC composite in 0.5 M HCl without and with Gt at varying temperatures

T (K)	C_{Inh} (mM)	R_{Ct} (Ωcm^2)	R_L (Ωcm^2)	R_p (Ωcm^2)	C_{dl} (μFcm^{-2})	% IE
303	Blank	11.48 ± 0.10	5.16 ± 0.05	3.56 ± 0.03	97.52 ± 0.94	-
	0.01	20.61 ± 0.20	12.66 ± 0.12	7.84 ± 0.07	35.83 ± 0.32	54.57
	0.05	28.57 ± 0.26	15.32 ± 0.14	9.97 ± 0.08	21.56 ± 0.20	64.27
	0.10	39.02 ± 0.28	20.23 ± 0.20	13.32 ± 0.13	14.98 ± 0.13	73.25
	0.25	43.26 ± 0.40	22.02 ± 0.19	14.59 ± 0.14	10.44 ± 0.09	75.58
	0.50	45.45 ± 0.39	23.65 ± 0.20	15.55 ± 0.14	9.97 ± 0.09	77.09
	0.75	49.07 ± 0.42	27.65 ± 0.22	17.68 ± 0.16	8.14 ± 0.07	79.85
313	Blank	7.22 ± 0.06	4.27 ± 0.04	2.68 ± 0.02	222.95 ± 2.23	-
	0.01	11.51 ± 0.09	7.34 ± 0.06	4.48 ± 0.04	95.46 ± 0.88	40.15
	0.05	16.95 ± 0.15	10.36 ± 0.10	6.43 ± 0.56	63.56 ± 0.62	58.28
	0.10	23.84 ± 0.30	14.45 ± 0.20	8.99 ± 0.24	40.97 ± 0.41	70.18
	0.25	27.68 ± 0.28	15.98 ± 0.24	10.13 ± 0.20	32.82 ± 0.31	73.52
	0.50	28.41 ± 0.22	17.32 ± 0.22	10.76 ± 0.24	27.74 ± 0.26	75.07
	0.75	29.84 ± 0.28	18.21 ± 0.26	11.31 ± 0.22	18.20 ± 0.17	76.28
323	Blank	3.91 ± 0.03	2.05 ± 0.01	1.34 ± 0.01	899.26 ± 8.88	-
	0.01	4.58 ± 0.04	4.11 ± 0.20	2.17 ± 0.02	281.63 ± 2.80	38.03
	0.05	7.33 ± 0.07	5.66 ± 0.16	3.15 ± 0.02	181.42 ± 1.79	57.29
	0.10	8.32 ± 0.07	6.07 ± 0.18	3.51 ± 0.03	145.03 ± 1.36	61.71
	0.25	9.99 ± 0.10	7.06 ± 0.20	4.14 ± 0.04	122.43 ± 1.20	67.53
	0.50	10.63 ± 0.11	7.61 ± 0.22	4.47 ± 0.04	103.09 ± 1.02	69.92
	0.75	11.95 ± 0.10	8.30 ± 0.24	4.89 ± 0.03	83.67 ± 0.82	72.56
333	Blank	3.50 ± 0.03	1.92 ± 0.02	1.24 ± 0.004	998.02 ± 9.35	-
	0.01	4.28 ± 0.03	3.52 ± 0.03	1.96 ± 0.006	402.06 ± 3.82	36.73
	0.05	6.22 ± 0.05	4.82 ± 0.04	2.72 ± 0.008	256.08 ± 2.42	54.41
	0.10	7.54 ± 0.06	5.52 ± 0.05	3.19 ± 0.018	182.16 ± 1.92	61.13
	0.25	8.62 ± 0.07	6.26 ± 0.06	3.63 ± 0.022	148.22 ± 1.38	65.84
	0.50	9.86 ± 0.09	6.88 ± 0.07	4.05 ± 0.024	126.18 ± 1.28	69.38
	0.75	10.54 ± 0.10	7.89 ± 0.08	4.43 ± 0.028	98.04 ± 1.12	72.00

Influence of temperature

The kinetic and thermodynamic data controlling the corrosion and inhibition process could be evaluated by studying the effect of temperature on *IE*. With the help of these parameters, one can follow the adsorption pattern of Gt molecules on the composite. As the temperature of the medium rises, the i_{corr} also increases because of the rise in the conductivity of the medium. In the presence of Gt, there is an increase in *IE,* revealing that the composite's deterioration is under control. PDP and EIS results (Tables 2 and 3) indicate the decline in *IE* observed with a temperature rise, showing the physisorption of Gt on the composite at higher temperatures [29].

The activation energy (E_a) for the corrosion of the composite specimen in 0.5 M HCl was computed as per the Arrhenius equation [30].

$$\ln(CR) = B - \frac{E_a}{RT} \tag{5}$$

The "B" indicates the Arrhenius constant, "R" is the gas constant (8.314 J K^{-1} mol^{-1}), and "T" is the temperature.

The slope of the straight line obtained (Fig. 6) by plotting ln (CR) versus 1/T is equal to $-E_a/R$. Thus, E_a values can be computed for the composite in the corrosive and inhibited corrosive medium.

The change in entropy ($\Delta S^{\#}$) and enthalpy ($\Delta H^{\#}$) of activation for the corrosion process in the acid and inhibited acid solution was computed as per the transition state equation [31].

$$CR = \frac{RT}{Nh} exp\left(\frac{\Delta S^{\#}}{R}\right) exp\left(\frac{-\Delta H^{\#}}{RT}\right) \tag{6}$$

In this relation, "N" is Avogadro's number (6.023 × 10^{23} mol^{-1}), and "h" denotes Planck's constant (6.626 × 10^{-34} J s).

The ln (CR/T) vs. 1/T plot (Fig. 7) gives a straight line with the slope and intercept value equal to ($-\Delta H^{\#}/R$) and [ln

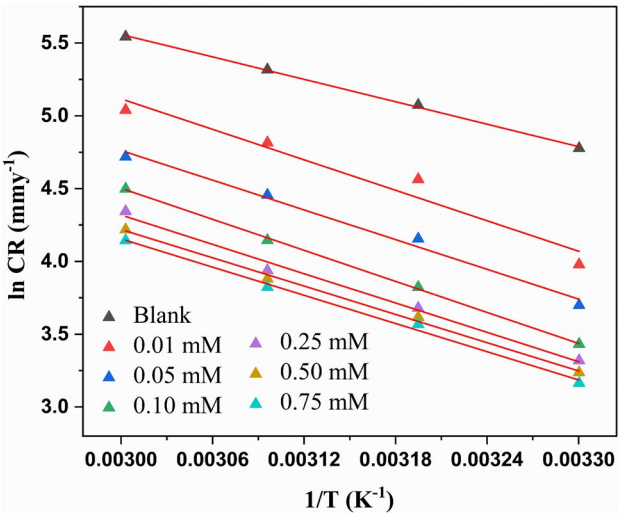

Fig. 6 Arrhenius plot for Al alloy-SiC composite in 0.5 M HCl without and with Gt

$(R/Nh)+\Delta S^{\#}/R]$, respectively. The activation parameters are recorded in Table 4.

E_a values in the inhibited acid medium were higher than in the acid medium (Table 4). The observed increase in E_a value in the inhibited acid medium suggests the physical adsorption of Gt on the composite [30]. Hence, the physically adsorbed Gt molecules can increase the physical energy barrier for the corrosion process. The surge in E_a value with an increase in Gt concentration may be due to the protective film formation by Gt molecules on the composite [15, 32]. The positive value of $\Delta H^{\#}$ indicates that the inhibition is an endothermic process. The $\Delta S^{\#}$ values are negative, showing the decrease in randomness occurring during the inhibition, favoring the adsorption of Gt molecules [33].

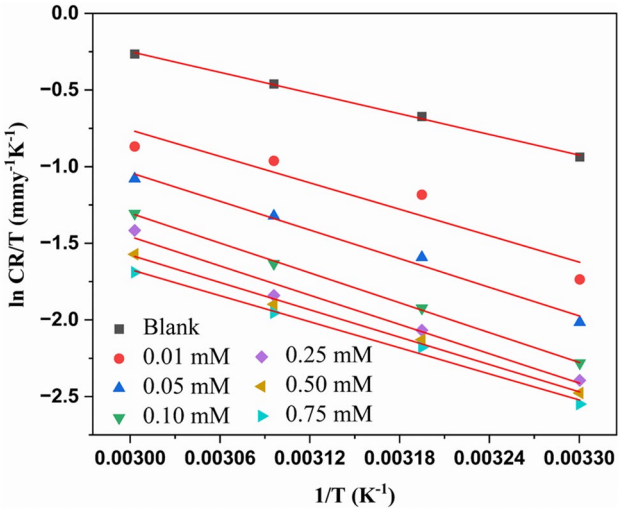

Fig. 7 ln(CR/T) versus 1/*T* plot for Al alloy-SiC in 0.5 M HCl without and with Gt

Table 4 The activation results for Al alloy-SiC composite in 0.5 M HCl without and with Gt

C_{Inh} (mM)	E_a (kJ mol^{-1})	R^2	$\Delta H^{\#}$ (kJ mol^{-1})	$\Delta S^{\#}$ (J mol^{-1} K^{-1})
Blank	21.35	0.9982	18.71	−143.46
0.01	29.00	0.9988	23.89	−132.17
0.05	28.29	0.9984	25.91	−128.42
0.10	29.54	0.9989	26.99	−127.38
0.25	27.93	0.9994	26.47	−130.20
0.50	26.92	0.9997	24.72	−136.47
0.75	26.83	0.9992	23.57	−140.71

Adsorption behavior of Gt

Organic inhibitors control metal corrosion by adsorption on the metal/medium interface, forming a protective coating that isolates the metal surface from the corrosive medium. The adsorption approach is commonly described as the process of displacement of water molecules adsorbed on the metal surface [$H_2O_{(ads)}$] by the organic inhibitor molecule in the aqueous medium [Inh(aq)] as indicated below [31]:

$$\mathrm{Inh}_{(aq)} + n\mathrm{H_2O}_{(ads)} \rightleftharpoons \mathrm{Inh}_{(ads)} + n\mathrm{H_2O}_{(aq)} \quad (7)$$

"n" is the number of water molecules displaced by the inhibitor molecules.

Adsorption mainly depends on the nature of the metal, the corrosive medium, the temperature of the medium, and the concentration and molecular structure of the inhibitor. The adsorption isotherm can provide the mode of interaction of inhibitors at the composite surface. The surface coverage (θ) values of Gt at different concentrations were obtained from PDP measurements. These results were applied to various isotherms. The adsorption isotherm with a linear regression coefficient (R^2) value close to one was carefully chosen as the best fit. In this case, the best linear fit was obtained with the Langmuir adsorption isotherm.

The Langmuir adsorption isotherm can be expressed by Eq. (8) [15]:

$$\frac{C_{Inh}}{\theta} = \frac{1}{K_{ads}} + C_{Inh} \quad (8)$$

where C_{Inh} denotes the inhibitor concentration, K_{ads} indicate the equilibrium constant for adsorption (mM^{-1}), and θ is the surface coverage, which is obtained by Eq. (9)

$$\theta = \frac{\%\,IE}{100} \quad (9)$$

$\%\ IE$ denotes the percentage inhibition efficiency obtained from Eq. (1).

The C_{Inh}/θ vs. C_{Inh} plot (Fig. 8) is a straight line whose intercept equals $1/K_{ads}$. The straight-line plot's regression

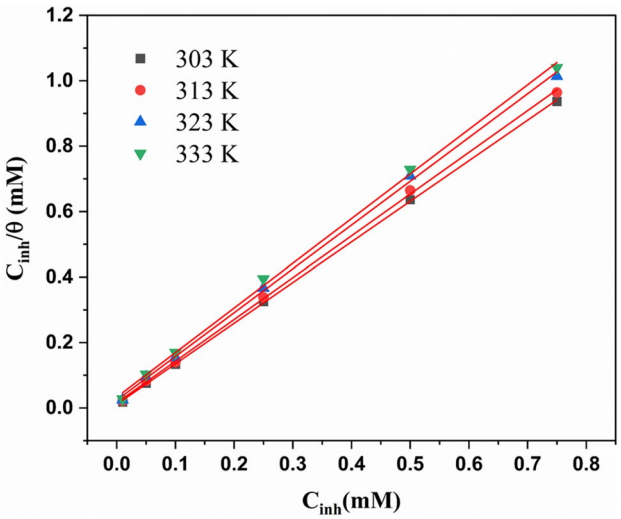

Fig. 8 C_{Inh}/θ vs. C_{Inh} plot for the adsorption of Gt on the composite surface

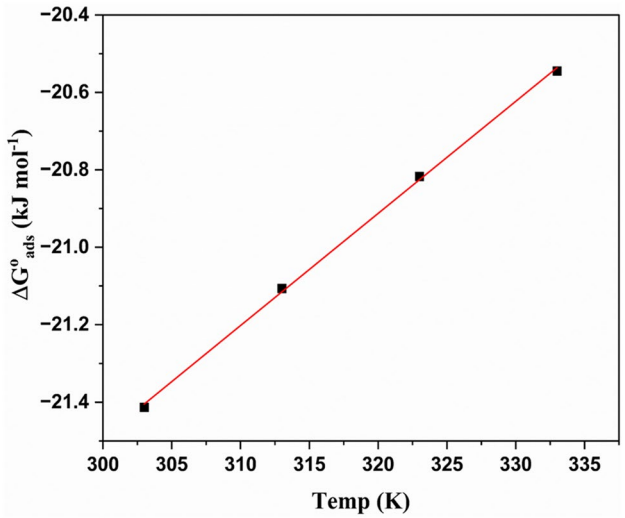

Fig. 9 ΔG^0_{ads} vs. T plot for the adsorption of Gt on the composite surface

coefficient (R^2) is much closer to unity, indicating that Langmuir's adsorption isotherm obeyed for the adsorption of Gt on the surface of the composite (Table 5). It suggests that the adsorbed Gt molecules form a monolayer film on the composite surface, and there is no interaction between the adsorbed Gt molecules.

The standard free energy of adsorption (ΔG^0_{ads}) value of Gt is related to its K_{ads} value according to Eq. (10) [34].

$$K_{ads} = \frac{1}{C_{water}} \exp\left(\frac{-\Delta G^0_{ads}}{RT}\right) \tag{10}$$

C_{water} indicates the molar concentration of water in the solution (55.5 mol/L).

The higher K_{ads} (Table 5) value reveals a strong interaction of Gt molecules at the composite surface, resulting in a higher *IE* [35]. Figure 9 depicts the ΔG^0_{ads} vs. T plot, representing a straight line. The standard adsorption value of enthalpy (ΔH^0_{ads}) and entropy (ΔS^0_{ads}) was equal to the slope and intercept of the straight line. The value of ΔG^0_{ads} is given by Eq. (11).

Table 5 Thermodynamic results for the adsorption of Gt on the composite surface

T (K)	K_{ads} (mM^{-1})	R^2	ΔG^0_{ads} (kJ mol^{-1})	ΔH^0_{ads} (kJ mol^{-1})	ΔS^0_{ads} (J mol^{-1} K^{-1})
303	88.574	0.9998	−21.41		
313	63.735	0.9996	−21.16	−30.17	−0.0289
323	41.911	0.9991	−20.82		
333	30.093	0.9980	−20.54		

$$\Delta G^0_{ads} = \Delta H^0_{ads} - T\Delta S^0_{ads} \tag{11}$$

The ΔG^0_{ads} value less than or equal to −20 kJ mol^{-1} suggests that the physisorption, while greater than or equal to −40 kJ mol^{-1}, indicates the chemisorption. ΔG^0_{ads} values between these threshold limits reveal the inhibitor's mixed adsorption on the composite surface [36]. As shown in Table 5, ΔG^0_{ads} values for Gt are in the range of −21 kJ mol^{-1}, and the values are closer to −20 kJ mol^{-1}, suggesting the mixed adsorption with stronger physisorption of Gt on the composite surface. A negative value of adsorption enthalpy indicates the inhibitor molecules' physical adsorption [37]. As reported, the ΔH^0_{ads} value for physisorption is lower than −41.86 kJ mol^{-1}, and for chemisorption, it must approach −100 kJ mol^{-1} [38]. The estimated value of ΔH^0_{ads} for Gt (Table 5) is −30.17 kJ mol^{-1}. It indicates that Gt molecules preferably undergo physisorption on the composite surface. The observed decrease in *IE* with the rise in temperature (Tables 2 and 3) supports the physisorption of Gt molecules [29]. Therefore, it may be concluded that the inhibitor follows mixed adsorption, with physisorption playing a significant role. The value of ΔS^0_{ads} is negative, showing decreased disorderliness during adsorption [39].

SEM and AFM analysis

Figure 10a depicts the SEM image of the Al alloy-SiC composite dipped in 0.5 M HCl, indicating a rough surface containing many cavities due to the aggressive action of the acid medium. The SEM image of the composite specimen (Fig. 10b) dipped in the corrosive medium added with 0.75 mM Gt showed a surface with fewer cavities. It may

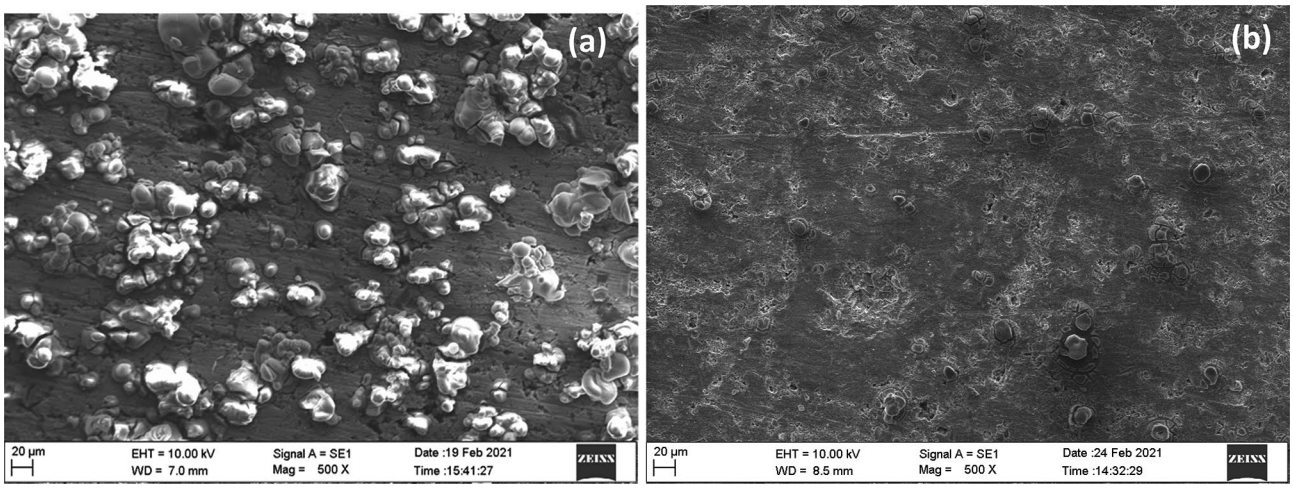

Fig. 10 The SEM pictures of composite samples dipped in 0.5 M HCl **a** without and **b** with 0.75 mM Gt

presumably be due to the adsorption of Gt molecules on the composite leading to a protective film. It blocks the further attack of the acid medium, controlling corrosion of the composite material.

The AFM pictures of the composite sample dipped in the corrosive medium without and with 0.75 mM Gt, respectively, are shown in Fig. 11a, b. The measured average values of surface roughness (R_a) and root mean square roughness (R_q) of the corroded and inhibited specimens are shown in Table 6. The measured roughness values, R_a and R_q, for the inhibited composite sample are lower than the corroded composite sample. The drastic reduction in the surface roughness on the inhibited specimen reveals the adsorption of Gt, controlling the deterioration of AA6061 in the HCl medium.

The proposed corrosion inhibition mechanism

Generally, an inhibitor controls the deterioration of a metal in contact with an acid medium by adsorbing its molecules over the metal surface. The inhibitor's adsorption behavior is governed by its nature, the inhibitor structure, the type of electrolyte, and temperature. In the HCl medium, aluminum corrosion occurs due to the depletion of the protective oxide layer. Aluminum with higher negative potential usually reacts with the hydrochloric acid medium and deteriorates following the anodic reactions [40]:

$$\mathrm{Al} + \mathrm{Cl}^- \rightleftarrows \mathrm{AlCl}^-_{\mathrm{ads}} \tag{12}$$

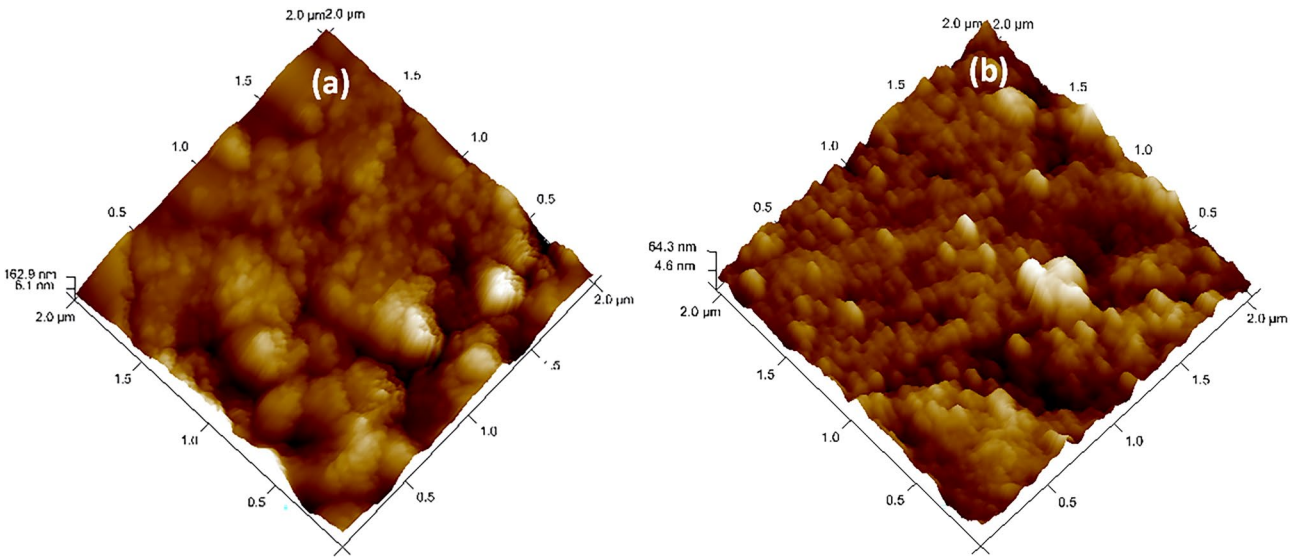

Fig. 11 The AFM images of the composite samples dipped in 0.5 M HCl **a** without and **b** with 0.75 mM of Gt

Table 6 The surface roughness results for Al alloy-SiC composite samples

Specimen	R_a (nm)	R_q (nm)
Composite dipped in 0.5 M HCl	57.6	78.2
Composite dipped in (0.5 M HCl + 0.75 mM)	11.4	15.2

$$AICl^-_{ads} + Cl^- \longrightarrow AICl^+_2 + 3e^- \quad (13)$$

The evaluation of hydrogen takes place at the cathode.

$$H^+ + e^- \longrightarrow H_{ads} \quad (14)$$

$$H_{ads} + H_{ads} \longrightarrow H_2 \quad (15)$$

Organic inhibitors can adsorb over the composite via physisorption, chemisorption, or both. As discussed earlier, Gt follows mixed-type adsorption predominantly with physisorption. In a strongly acidic medium, Al alloy-SiC composite surface can attain a positive charge since the value of pH_{zch} (i.e., pH at zero charge potential) for aluminum is 9.1 [41]. As a result, the chloride ions first adsorb by the electrostatic force of attraction at the composite/HCl solution interface. Hence, the composite surface acquires a negative charge. Being an amino acid derivative, Gt can undergo protonation in an acid medium similar to the one used in the present work [40]. The negatively charged composite surface can easily attract the protonated inhibitor, leading to physisorption (Fig. 12). The chemisorption of Gt can occur by sharing electron pairs on N, S, O atoms, and π-electrons of carbonyl groups in Gt with the empty *d*-orbitals of aluminum, leading to a coordination bond (Fig. 12) [42]. As reported elsewhere, electron-donating groups (−OH, $-NH_2$) can improve the inhibitive performance of Gt [43].

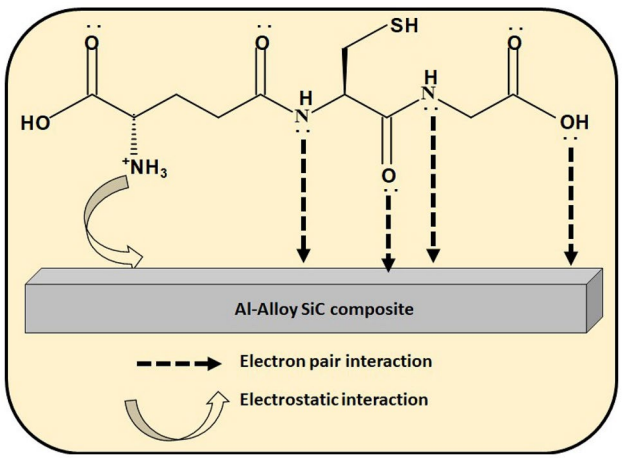

Fig. 12 Adsorption pattern for Gt on the composite surface

UV–visible and FTIR analysis on adsorption of Gt

The adsorption of Gt molecules on the Al alloy-SiC composite surface can be confirmed using UV–visible spectra. The UV–vis spectra of 0.1 mM Gt in 0.5 M HCl solution (Fig. 13) revealed two absorption peaks (228 and 290 nm), corresponding to the π → π* and n → π* transitions, respectively. The composite specimen was immersed for 2 h in 0.1 mM Gt in 0.5 M HCl solution, and UV–vis spectra were retaken. The second recorded spectra had the same two peaks as the first, but their intensity was lower. The decrease in the intensity of the second spectra supports the adsorption of Gt molecules on the composite surface.

The FTIR spectra of Gt are shown in Fig. 14. The observed FTIR absorption peaks are (ATR, cm^{-1}) around 3200 (OH, NH_2, NH *str.*), 2520 (SH, *str.*), 1700 (C=O *str.* of COOH), and 1514 (C=O *str.* of amide). The scraped corrosion product obtained from the specimen composite after immersing in 0.5 M HCl solution containing 0.1 mM Gt for 2 h showed the same peaks but with less intensity, confirming the physisorption of Gt molecules on the composite surface.

Theoretical DFT analysis

As per the DFT-based theoretical calculations, different parameters were evaluated to understand the interaction of the inhibitor on the composite metal surface. Gt can exist in the protonated form in an aqueous acid medium [41, 44]. Since the composite is exposed to an acidic medium (0.5 M HCl), the participation of protonated Gt could not be ruled out along with neutral Gt in the corrosion inhibition process.

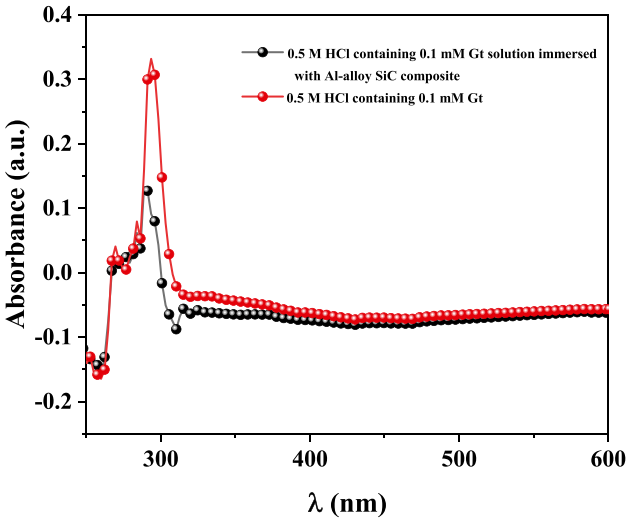

Fig. 13 UV–visible spectra of 0.1 mM Gt in 0.5 M HCl before and after immersion of composite specimen

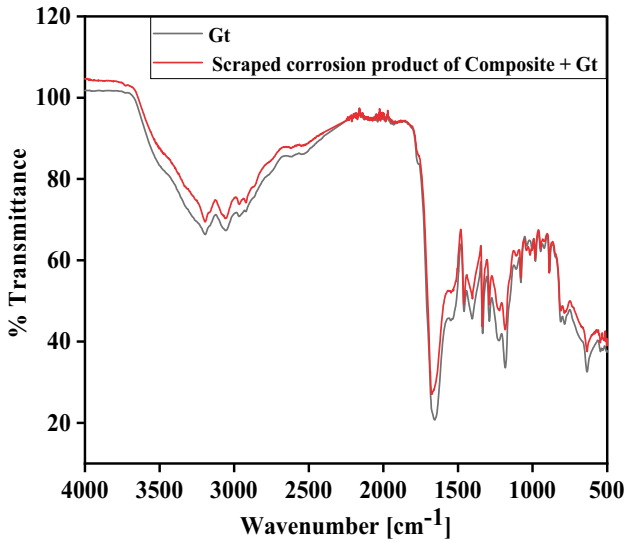

Fig. 14 FTIR spectra of Gt and scraped corrosion product

Hence, the DST calculations using the 6-31G** basis set were carried out on neutral and protonated Gt.

Figures 15a–f depict the optimized structure and the frontier molecular orbital structures of neutral and protonated Gt.

The E_{HOMO} and E_{LUMO} values are interrelated to the value of I (ionization potential) and A (electron affinity), respectively, as per the relations, Eqs. (16) and (17) [45].

$$I = -E_{HOMO} \tag{16}$$

$$A = -E_{LUMO} \tag{17}$$

The values of χ, η, and σ were computed using Eqs. (18–20), respectively [45, 46].

$$\chi = \frac{I + A}{2} \tag{18}$$

$$\eta = \frac{I - A}{2} \tag{19}$$

$$\sigma = \frac{1}{\eta} \tag{20}$$

The ΔN involved in the inhibitor and metal surface interaction was obtained using Eq. (21) [47].

$$\Delta N = \frac{X_{Al} - X_{Inh}}{2(\eta_{Al} + \eta_{Inh})} = \frac{\Phi_{Al} - X_{Inh}}{2\eta_{Inh}} \tag{21}$$

In these relations, χ_{Al} and χ_{Inh} represent the electronegativity, while η_{Al} and η_{Inh} indicate the hardness of Al and inhibitor, respectively, and ϕ_{Al} is the work function. In the present work for aluminum, the theoretical value of electronegativity, ϕ_{Al}, is taken as 4.28 eV [48] and η_{Al} as zero [47].

As per Parr et al. [49], the electrophilicity index (ω) is given by Eq. (22):

$$\omega = \frac{\mu^2}{2\eta} \tag{22}$$

In the above relation, μ indicates the electronic chemical potential, defined as:

$$-\mu = \frac{I + A}{2} = \chi \tag{23}$$

The parameters like energies of the highest occupied molecular orbital (E_{HOMO}) and lowest unoccupied molecular orbital (E_{LUMO}), energy gap (ΔE_g), hardness (η) and softness (σ), the fraction of transferred electrons (ΔN), and the electrophilicity index (ω) are summarized in Table 7.

The Gt molecule has multiple heteroatoms (O, N, S). Therefore, the heteroatoms in Gt with high negative Mulliken charges can preferably act as the active sites of adsorption. Figure 16a, b reveals that the heteroatoms such as N6 (−0.58), O10 (−0.55), N14 (−0.53), N10 (−0.53), O15 (−0.52), N9 (−0.52), O1 (−0.47), O18 (−0.47), O19 (−0.46), and O4 (−0.46) in neutral Gt molecule show high negative charges. Similarly in protonated Gt heteroatoms such as N6 (−0.56), O10 (−0.52), N14 (−0.51), N9 (−0.52), O19 (−0.52), N14 (−0.51), O15 (−0.51), O1 (−0.45), O4 (−0.45), and O18 (−0.43) show high negative Mulliken charges. These heteroatoms can provide active sites for adsorption.

Generally, the value of E_{HOMO} indicates the inhibitor's electron-releasing tendency. A larger E_{HOMO} value of the inhibitor indicates its higher electron-releasing and lower electron-accepting capability. The value of E_{LUMO} reveals the electron-accepting property. The inhibitors with lower values of E_{LUMO} exhibit poor electron-realizing properties

Table 7 Quantum chemical parameters for neutral and protonated Gt

Property	Neutral Gt	Protonated Gt
E_{HOMO}	−6.6472 eV	−9.1653 eV
E_{LUMO}	−0.2373 eV	−4.2472 eV
ΔE_g	6.4099 eV	4.9181 eV
I	6.6472 eV	9.1653 eV
A	0.2373 eV	4.2472 eV
χ	3.4422 eV	6.7062 eV
η	3.2949 eV	2.4590 eV
σ	0.3035 eV	0.4066 eV
ω	1.7983	9.1445
ΔN	0.1271	−0.4933

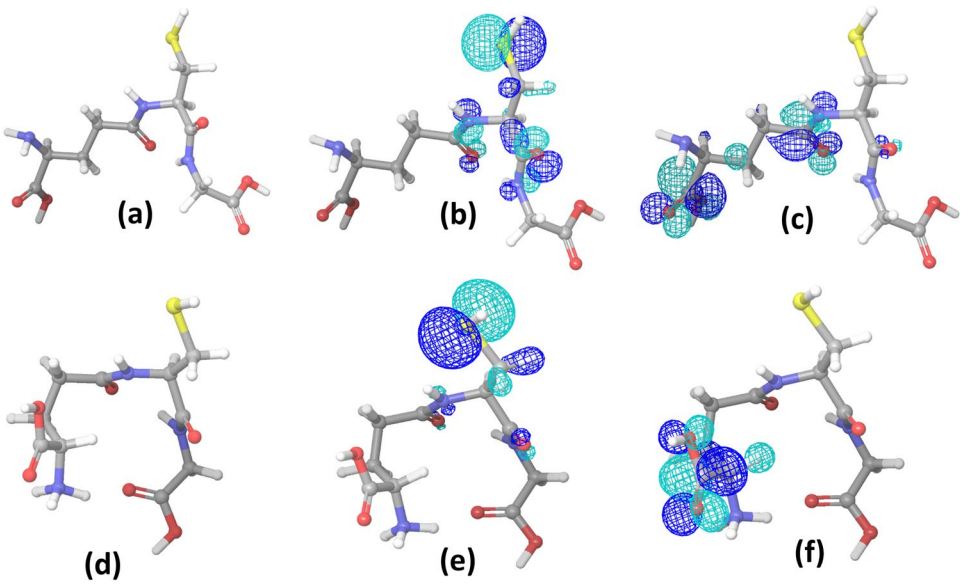

Fig. 15 Neutral Gt—**a** optimized structure, **b** HOMO, and **c** LUMO. Protonated Gt—**d** optimized structure, **e** HOMO, and **f** LUMO

and a more robust electron-accepting nature [50]. It is evident (Table 7) that neutral Gt shows a higher E_{HOMO} value (−6.6472 eV) compared to protonated Gt (−9.1653 eV). It reveals that neutral Gt exhibits better electron-releasing properties than its protonated species. E_{LUMO} value of protonated Gt is lower (−4.2472 eV) than neutral Gt (−0.2373 eV), which indicates the former's better electron-accepting tendency.

The energy bandgap (ΔE_g) between the HOMO and LUMO can predict inhibitor species' relative adsorption order. In general, higher chemical reactivity is shown by the inhibitor species with lower ΔE_g value and, hence, exhibits high inhibition activity [51]. In this work, the ΔE_g value for protonated Gt (4.9181 eV) is lower than neutral Gt (6.4099 eV). Hence, protonated Gt can show higher reactivity and good inhibition performance. It supports the physisorption of Gt on the composite surface, as revealed by the experimental results. According to the HSAB principle, chemical hardness and softness parameters influence the inhibition performance of the inhibitor molecule. The bulk metals are chemically soft and preferentially interact strongly with soft inhibitor species. The inhibitor species with a lower η value and higher σ value imply stronger chemical reactivity and contribute more towards *IE* [52]. In the present case, protonated Gt showed this behavior, indicating its good inhibition activity. Once again, this confirmed the physisorption of protonated Gt.

The value of $\Delta N > 0$ reveals the greater electron-donating tendency of inhibitor species, while $\Delta N < 0$ shows the higher electron-accepting trend [53]. Table 7 indicates that neutral Gt can readily donate electrons, and protonated Gt can accept electrons. A good nucleophile exhibits a low value of ω, whereas a good electrophile exhibits a high value of ω [54]. The protonated Gt showed the highest ω value (9.1445),

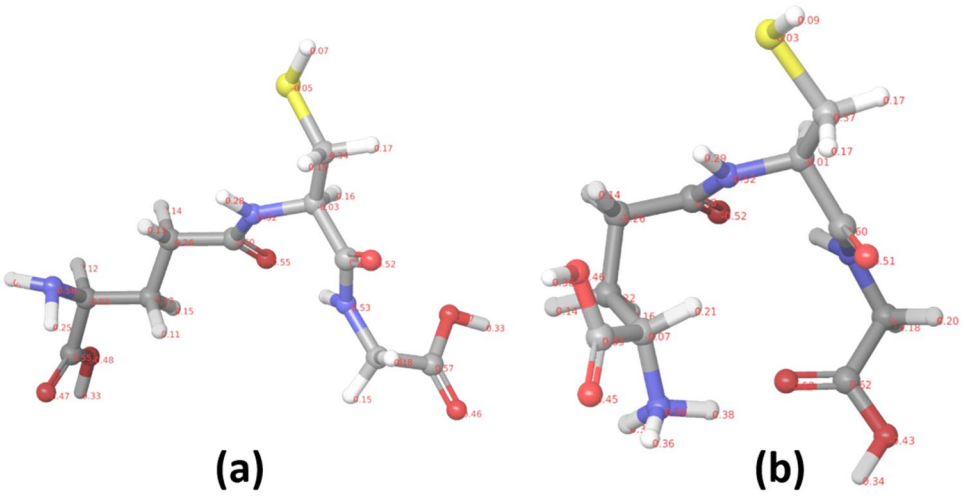

Fig. 16 Mulliken charges on atoms of **a** neutral and **b** protonated Gt

indicating its higher tendency to accept electrons from composite metal. It results in stronger adsorption of protonated Gt on the composite, improving the *IE*.

Conclusions

The following key features can be summarized based on experimental, theoretical, spectral, and surface analysis results.

The electrochemical results proved Gt as a potential green inhibitor for attenuating Al alloy-SiC composite corrosion in a 0.5 M HCl medium. The inhibitor, Gt, showed a mixed inhibitor behavior that significantly influenced the cathodic reactions. Gt evinced inhibition efficiency of 80% by PDP and EIS methods at a concentration of 0.75 mM and 303 K temperature. Thermodynamic results revealed the mixed adsorption of Gt with stronger physisorption on the composite surface. The adsorption of Gt on the composite surface follows the Langmuir adsorption isotherm. The electrochemical results show that the inhibition efficiency increases with a rise in medium temperature, suggesting the physical adsorption mode of Gt on the composite. The surface morphology analysis by SEM and AFM studies provides evidence for the protective film formation by the adsorption of Gt molecules on the composite surface. The results of the EIS technique support the PDP results. The spectral (UV–visible and FTIR) analysis confirmed the adsorption of Gt molecules on the composite surface. The theoretical studies using DFT validate the experimental results. Gt acts as an efficient inhibitor for Al alloy-SiC composite in HCl medium owing to its potential attributes like bulky molecular size, multiple donor atoms (N, S, and O), water solubility, stability, and ready availability with reasonable cost and non-toxic nature.

Acknowledgements The authors thank the Manipal Institute of Technology, Manipal Academy of Higher Education, Manipal, for the laboratory facilities.

Funding Open access funding provided by Manipal Academy of Higher Education, Manipal

Declarations

Competing interests The authors declare no competing interests.

References

1. Revie RW, Uhlig HH (2008) Corrosion and corrosion control-an introduction to corrosion science and engineering. John Wiley & Sons Inc, New Jersey
2. Foltz JW (1999) In: Davis JW (ed) Metal-matrix composites, Vol. 2, ASM International, Materials Park, OH
3. Prasad SV, Asthana R (2014) Aluminium metal-matrix composites for automotive applications: Tribological considerations. Tribol Lett 17:445–453. https://doi.org/10.1023/B:TRIL.0000044492.91991.f3
4. Bobic B, Mitrovic S, Bobic M, Bobic I (2010) Corrosion of metal-matrix composites with aluminium alloy substrate. Tribol Ind 32:3–11
5. Xhanari K, Finsgar M (2016) Organic corrosion inhibitors for aluminium and its alloys in acid solutions: a review. RSC Aadv 6:62833–62857. https://doi.org/10.1039/C6RA11818F
6. Shetty P (2018) Hydrazide derivatives: an overview of their inhibition activity against acid corrosion of mild steel. S Afr J Chem 71:46–50. https://doi.org/10.17159/0379-4350/2018/v71a6
7. Hamadi L, Mansouri S, Oulmi K, Kareche A (2018) The use of amino acids as corrosion inhibitors for metals: a review. Egypt J Pet 27(4):1157–1165. https://doi.org/10.1016/j.ejpe.2018.04.004
8. Zhang D-Q, Cai Q-R, He X-M, Gao L-X, Kim GS (2009) The corrosion inhibition of copper in hydrochloric acid solutions by a tripeptide compound. Corros Sci 51:2349–2354. https://doi.org/10.1016/j.corsci.2009.06.015
9. Nagalaxmi, Shetty P, Kumari PP (2020) Inhibitive action of glutathione reduced on the deterioration of AA6061 in 0.5M HCl. Tribol Ind 42:214–224. https://doi.org/10.24874/ti.785.10.19.02
10. Brett CMA (1992) On the electrochemical behavior of aluminium in acidic chloride solution. Corros Sci 33:203–210
11. Musa AY, Mohamad AB, Kadhum AAH, Chee EP (2011) Galvanic corrosion of aluminium alloy (Al2024) and copper in 1.0 M nitric acid. Int J Electrochem Sci 6:5052–5065
12. Wh LI, He Q, Pei CL, Hou BR (2007) Experimental and theoretical investigation of the adsorption behavior of new triazole derivatives as inhibitors for mild steel corrosion in acid media. Electrochim Acta 52:6386–6394. https://doi.org/10.1016/j.electacta.2007.04.077
13. Arukalam IO, Imadu IO, Ijomah NT, Ewulonu CM, Onyeagoro GN (2014) Acid corrosion inhibition and adsorption behavior of ethyl hydroxyethyl cellulose on mild steel corrosion. J Mater 2014:101709. https://doi.org/10.1155/2014/101709
14. Fontana MG (1987) Corrosion engineering, 3rd edn. McGraw-Hill, Singapore
15. Khaled KF, Al-Qahtani MM (2009) The inhibitive effect of some tetrazole derivatives towards Al corrosion in acid solution: Chemical, electrochemical and theoretical studies. Mater Chem Phys 13:150–158. https://doi.org/10.1016/j.matchemphys.2008.07.060
16. Ahamed I, Quraishi MA (2009) Bis (benzimidazol-2-yl) disulphide: an efficient water soluble inhibitor for corrosion of mild steel in acid media. Corros Sci 51:2006–2013. https://doi.org/10.1016/j.corsci.2009.05.026
17. Metikos-Hukovic M, Babic R (1998) Corrosion protection of aluminium in acidic chloride solutions with non-toxic inhibitors. J Appl Electrochem 28:433–439
18. Noor EA (2008) Evaluation of inhibitive action of some quaternary N-heterocyclic compounds on the corrosion of Al–Cu alloy in hydrochloric acid. Mater Chem Phys 114:533–541. https://doi.org/10.1016/j.matchemphys.2008.09.065

19. Pinto GM, Nayak J, Shetty AN (2011) Corrosion inhibition of 6061 Al–15 vol. pct. SiC(p) composite and its base alloy in a mixture of sulphuric acid and hydrochloric acid by 4-(N, N-dimethyl amino) benzaldehyde thiosemicarbazone. Mater Chem Phys 125:628–640. https://doi.org/10.1016/j.matchemphys.2010.10.006
20. Kumari PP, Shetty P, Nagalaxmi DS (2020) Effect of cysteine as environmentally friendly inhibitor on AA6061-T6 corrosion in 0.5 M HCl: electrochemical and surface studies. Surf Eng Appl Electrochem 56:624–634. https://doi.org/10.3103/S1068375520050087
21. Metikos-Huković M, Babic R, Grubac Z (1998) Corrosion protection of aluminium in acidic chloride solutions with non-toxic inhibitors. J Appl Electrochem 28:433–439. https://doi.org/10.1023/A:1003200808093
22. Pinto GM, Nayak J, Shetty AN (2011) Adsorption and inhibitor action of 4-(N, Ndimethylamino) benzaldehyde thiosemicarbazone on 6061 Al SiC composite and its base alloy in sulfuric acid medium. Synth React Inorg M 41:37–41. https://doi.org/10.1080/15533174.2010.538023
23. Ansari KR, Yadav DK, Ebenso EE, Quraishi MA (2012) Novel and effective pyridyl substituted 1,2,4-triazole as corrosion inhibitor for mild steel in acid solution. Int J Electrochem Sci 7:4780–4799
24. Eid S, Abdallah M, Kamar EM (2015) Corrosion inhibition of aluminium and aluminium silicon alloys in sodium hydroxide solutions by methylcellulose. J Mater Environ Sci 6:892–901
25. Ravari FB, Dadgareenezhad A (2013) Synergistic influence of propargyl alcohol and zinc sulfate on inhibition of corrosion of aluminium in 0.5 M H_2SO_4. J Chil Chem Soc 58:1853–1857. https://doi.org/10.4067/S0717-97072013000300013
26. Shetty KS, Shetty AN (2017) Eco-friendly benzimidazolium based ionic liquid as a corrosion inhibitor for aluminum alloy composite in acidic media. J Mol Liq 225:426–438. https://doi.org/10.1016/j.molliq.2016.11.037
27. Lebrini M, Lagrenée M, Vezin H, Traisnel M, Bentiss F (2007) Experimental and theoretical study for corrosion inhibition of mild steel in normal hydrochloric acid solution by some new macrocyclic polyether compounds. Corros Sci 49(2007):2254–2269. https://doi.org/10.1016/j.corsci.2006.10.029
28. Bentiss F, Traisnel M, Lagrenee M (2000) The substituted 1,3,4-oxadiazoles: a new class of corrosion inhibitors of mild steel in acidic media. Corros Sci 42:127–146. https://doi.org/10.1016/S0010-938X(99)00049-9
29. Abd El Rehim SS, Hassan HH, Amin MA (2002) The corrosion inhibition study of sodium dodecyl benzene sulphonate to aluminium and its alloys in 1.0 M HCl solution. Mater Chem Phys 78:337–348. https://doi.org/10.1016/S0254-0584(01)00602-2
30. Schorr M, Yahalom J (1972) The significance of the energy of activation for the dissolution reaction of metal in acids. Corros Sci 12:867–868. https://doi.org/10.1016/S0010-938X(72)80015-5
31. Abdel Rehim SS, Ibrahim MAM, Khaled KF (1999) 4-Aminoantipyrine as an inhibitor of mild steel corrosion in HCl solution. J Appl Electrochem 29:593–599. https://doi.org/10.1023/A1003450818083
32. Martinez S, Stern I (2002) Thermodynamic characterization of metal dissolution and inhibitor adsorption processes in the low carbon steel/mimosa tannin/sulfuric acid system. Appl Surf Sci 199:83–89. https://doi.org/10.1016/S0169-4332(02)00546-9
33. Singh AK, Quraishi MA (2011) Investigation of the effect of disulfiram on corrosion of mild steel in hydrochloric acid solution. Corros Sci 53:1288–1297. https://doi.org/10.1016/j.corsci.2011.01.002
34. Bayol E, Kayakırılmaz K, Erbil M (2007) The inhibitive effect of hexamethylene tetramine on the acid corrosion of steel. Mater Chem Phys 04:74–82. https://doi.org/10.1016/j.matchemphys.2007.02.073
35. Tang L, Li X, Si Y, Mu G (2006) The synergistic inhibition between 8-hydroxy quinoline and chloride ion for the corrosion of cold rolled steel in 0.5 M sulfuric acid. Mater Chem Phys 95:29–38. https://doi.org/10.1016/j.matchemphys.2005.03.064
36. Nnanna LA, Onwuagba BN, Mejeha IM, Okeoma KB (2010) Inhibition effects of some plant extracts on the acid corrosion of aluminium alloy. Afr J Pure Appl Chem 4:11–16
37. Ahamad I, Prasad R, Quraishi MA (2010) Thermodynamic, electrochemical and quantum chemical investigation of some Schiff bases as corrosion inhibitors for mild steel in hydrochloric acid solutions. Corros Sci 52:933–942. https://doi.org/10.1016/j.corsci.2009.11.016
38. Quraishi MA, Rawat J, Ajmal M (2000) Dithiobiurets: a novel class of acid corrosion inhibitors for mild steel. J Appl Electrochem 30:745–751. https://doi.org/10.1023/A:1004099412974
39. Bentiss F, Traisnel M, Lagrenee M (2001) Influence of 2,5-bis(4-dimethylaminophenyl)-1,3,4-thiadiazole on corrosion inhibition of mild steel in acidic media. J Appl Electrochem 31:41–48. https://doi.org/10.1023/A:1004141309795
40. Bereket G, Pinarbsi A (2004) Electrochemical thermodynamic and kinetic studies of the behaviour of aluminium in hydrochloric acid containing various benzotriazole derivatives. Corros Eng Sci Technol 39:308–312. https://doi.org/10.1179/174327804X13136
41. Bereket G, Yurt A (2001) The inhibition effect of amino acids and hydroxyl carboxylic acids on pitting corrosion of aluminium alloy 7075. Corros Sci 43:1179–1195. https://doi.org/10.1016/S0010-938X(00)00135-9
42. McCafferty E (2010) Introduction to corrosion science. Springer, New York
43. Verma C, Olasunkanmi LO, Ebenso EE, Quraishi MA (2018) Substituents effect on corrosion inhibition performance of organic compounds in aggressive ionic solutions: a review. J Mol Liq 251:100–118. https://doi.org/10.1016/j.molliq.2017.12.055
44. Yurt A, Bereket G, Ogretir C (2005) Quantum chemical studies on inhibition effect of amino acids and hydroxy carboxyic acids on pitting corrosion of aluminium alloy 7075 in NaCl solution. J Mol Struct: THEOCHEM 725:215–221. https://doi.org/10.1016/j.theochem.2005.01.048
45. Zhan CC, Nichols JA, Dixon DA (2003) Ionization potential, electron affinity, electronegativity, hardness, and electron excitation energy: Molecular properties from density functional theory orbital energies. J Phys Chem A 107:4184–4195. https://doi.org/10.1021/jp0225774
46. Pearson RG (1988) Absolute electronegativity and hardness: Application to inorganic chemistry. Inorg Chem 27:734–740. https://doi.org/10.1021/ic00277a030
47. Pearson RG (1990) Hard and soft acids and bases-the evolution of a chemical concept. Coord Chem Rev 100C:403–425
48. Kokalj A, Kovacevic N (2011) On the consistent use of electrophilicity index and HSAB-based electron transfer and its associated change of energy parameters. Chem Phys Lett 507:181–184. https://doi.org/10.1016/j.cplett.2011.03.045
49. Parr RG, Szentpal LV, Liu YS (1922) Electrophilicity index. J Am Chem Soc 121:1922–1924
50. Keles H, Keles M, Dehri I, Serindag O (2008) The inhibitive effect of 6-amino-m-cresol and its Schiff base on the corrosion of mild steel in 0.5M HCI medium. Mater Chem Phys 112:173–179. https://doi.org/10.1016/j.matchemphys.2008.05.027
51. Ahamad I, Prasad R, Quraishi MA ((2010) Experimental and quantum chemical characterization of the adsorption of some Schiff base compounds of phthaloyl thiocarbohydrazide on the mild steel in acid solutions. Mater Chem Phys 124:1155–1165. https://doi.org/10.1016/j.matchemphys.2010.08.051
52. Masoud MS, Awad MK, Shaker MA (2010) The role of structural chemistry in the inhibitive performance of some amino pyrimidines on the corrosion of steel. Corros Sci 52:2387–2396. https://doi.org/10.1016/j.corsci.2010.04.011

53. Dahiya S, Saini N, Dahiya N (2018) Corrosion inhibition activity of an expired antibacterial drug in acidic media amid elucidate DFT and MD simulations. Port Electrochem Acta 36:13–230. https://doi.org/10.4152/pea.201803213
54. Obot IB, Obi-Egbedi NO (2010) Adsorption properties and inhibition of mild steel corrosion in sulphuric acid solution by ketoconazole: experimental and theoretical investigation. Corros Sci 52:198–204. https://doi.org/10.1016/j.corsci.2009.09.002